

# Divergent resistance at the Dirac point in graphene: Evidence for a transition in a high magnetic field

Joseph G. Checkelsky, Lu Li and N. P. Ong

Department of Physics, Princeton University, Princeton, NJ 08544, USA

(Dated: February 20, 2024)

We have investigated the behavior of the resistance of graphene at the  $n = 0$  Landau Level in an intense magnetic field  $H$ . Employing a low-dissipation technique (with power  $P < 3 \text{ fW}$ ), we find that, at low temperature  $T$ , the resistance at the Dirac point  $R_0(H)$  undergoes a 1000-fold increase from  $10 \text{ k}$  to  $40 \text{ M}$  within a narrow interval of field. The abruptness of the increase suggests that a transition to an insulating, ordered state occurs at the critical field  $H_c$ . Results from 5 samples show that  $H_c$  depends systematically on the disorder, as measured by the offset gate voltage  $V_0$ . Samples with small  $V_0$  display a smaller critical field  $H_c$ . Empirically, the steep increase in  $R_0$  fits accurately a Kosterlitz-Thouless-type correlation length over 3 decades. The curves of  $R_0$  vs.  $T$  at fixed  $H$  approach the thermal-activation form with a gap  $\sim 15 \text{ K}$  as  $H \rightarrow H_c$ , consistent with a field-induced insulating state.

PACS numbers: 73.63.-b, 73.21.-b, 73.43.-f

## I. INTRODUCTION

In graphene, the low energy states display a linear energy-momentum dispersion described by the Dirac Hamiltonian. The observation of the integer quantum Hall (QH) effect by Novoselov et al. [1, 2, 3] and Zhang et al. [4, 5, 6] has sparked intense interest in this novel 2D (two-dimensional) system. In a strong magnetic field  $H$ , the states are quantized into Landau Levels. As a result of the Dirac dispersion, the energy  $E_n$  of the Landau Level (LL) (of index  $n$ ) increases with the flux density  $B$  as  $E_n \sim \text{sgn}(n) \frac{2e\hbar v_F}{2} B |n|$ , where  $v_F$  is the Fermi velocity,  $e$  the electron charge, and  $\hbar$  is Planck's constant. The Hall conductivity is observed to be accurately quantized as  $\sigma_{xy} = (4e^2/\hbar) [n + \frac{1}{2}] = 2e^2/\hbar$ , where  $e$  is the electron charge,  $2\pi\hbar$  is Planck's constant, and  $n$  the sublevel index. A key question is the nature of the ground state at the Dirac point. In intense  $H$ , theory predicts interesting broken-symmetry states driven by exchange and interaction. These are characterized as quantum Hall ferromagnetism (QHF) [7, 8, 9, 10, 11, 12], or excitonic condensation [13, 14, 15, 16]. These collective states imply the existence of field-induced phase transitions, but the experimental situation is rather unsettled. Moreover, the proposed [12, 17, 18] existence of counter-propagating edge modes at the Dirac point has further enriched the theoretical debate. Is the high-field Dirac point a QH insulator or a QH metal?

Recently, we reported [19] that the resistance at the Dirac point  $R_0$  begins to increase steeply at  $B = 10\text{-}12 \text{ T}$ , suggesting a transition to an insulating state. However, the results left open several key questions. Because  $R_0$  increased by only 1-decade (to  $0.2 \text{ M}$ ) [19], we could not establish that the high-field state is truly insulating. In graphene, the extreme sensitivity to thermal runaway has been highly problematic for researching its high- $H$  ground state [5, 6, 19]. Adopting a low-dissipation technique to avoid self-heating, we have measured the divergence in  $R_0$  to  $40 \text{ M}$  ( $\sim 1500 \text{ h} = e^2$ ) in 3 samples.

Remarkably, the divergence is accurately described over 3 decades by the Kosterlitz-Thouless (KT) correlation length. The singular nature of the divergence provides strong evidence that a 2D transition to an insulating state occurs when  $B$  exceeds a critical field  $H_c$ . The systematic variation of  $H_c$  with  $|V_0|$  (the gate voltage needed to bring the chemical potential to the Dirac point) implies that disorder is very effective in delaying  $H_c$  to higher field values. In all samples investigated to date, the transition to the insulating state is reached in fields below  $35 \text{ T}$ .

## II. EXPERIMENTAL DETAILS

Empirically, problems associated with self-heating in graphene become serious when the power dissipated  $P$  exceeds  $10 \text{ pW}$  for bath temperature  $T_b < 1 \text{ K}$ . As discussed in the Appendix, self-heating below  $1 \text{ K}$  leads to a number of spurious features caused by thermal instability in the sample. We adopted a simple voltage-controlled technique with ultra-low dissipation that avoids this difficulty, and allows the divergence in  $R_0$  to be measured reliably to  $40 \text{ M}$ . An ac source maintains a fixed voltage amplitude ( $40 \text{ V}$ ) across the sample in series with a  $100\text{-k}$  resistor (details are given in the Appendix). By phase-sensitive detection of both the current  $I$  and the voltage  $V_{xx}$ , we have made 4-probe measurements of  $R_0$  with ultra-low dissipation ( $P$  decreases from  $3 \text{ fW}$  at  $10 \text{ T}$  to  $40 \text{ aW}$  above  $25 \text{ T}$ ). Moreover, for  $T < 1.5 \text{ K}$ , the sample is immersed in liquid  $^3\text{He}$  so that the electrons in graphene are in direct contact with the bath. The largest reliably measured  $R_0$  is now  $40 \text{ M}$  (limited by the input impedance  $100 \text{ M}$  of the preamplifier). The new results provide an enlarged view of the interesting region in which  $R_0$  diverges. The samples K52 and J24 have offset voltages  $V_0$  much larger than that in K7, the sample investigated in detail in Ref. [19]. All samples except J18 were measured as-fabricated. Sample J18 was subject to a  $\frac{1}{2}$  hr. anneal in He gas at  $80 \text{ C}$  which decreased  $V_0$  to

8 V. However its large  $H_c$  suggests that its initial value of  $V_0$  (before annealing) is very large.

In Samples K 52, J18 and J24, the spacings between voltage leads are 3.5, 2.75 and 3  $\mu\text{m}$ , while the widths are 3, 3 and 2  $\mu\text{m}$ , respectively.

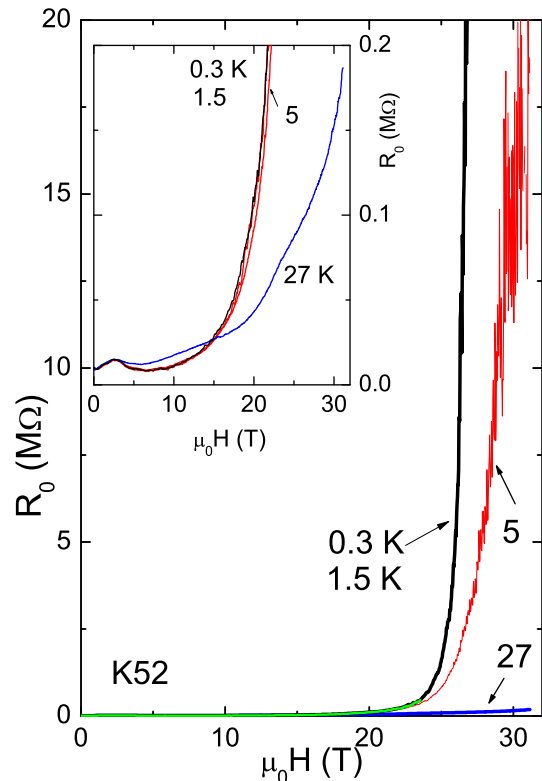


FIG. 1: (color online) (Main Panel) Divergence of the resistance  $R_0$  at the Dirac point with  $B$  at  $T = 0.3, 1.5, 5$  and  $27$  K (Sample K 52). At  $27$  K, the increase in  $R_0$  is quite moderate (to  $190$  k  $\Omega$  at  $H = 31$  T). At  $T = 0.3$  K, however,  $R_0$  exceeds  $20$  M  $\Omega$  above  $27$  T. The curves at  $0.3$  and  $1.5$  K undergo a 1000-fold increase ( $40$  k  $\Omega$  to  $40$  M  $\Omega$ ) in the narrow field interval  $17$ - $27$  T. In high  $B$ , the  $5$  K curve deviates significantly from them. The inset shows the behavior of  $R_0$  vs.  $H$  in greatly expanded scale ( $\times 100$ ). The voltage-regulated technique used for these measurements dissipates  $3$   $\mu\text{W}$  at  $10$  T and  $40$   $\mu\text{W}$  above  $25$  T.

### III. FIELD DEPENDENCE OF $R_0$

Figure 1 (main panel) shows curves of  $R_0$  vs.  $H$  in K 52 at temperatures  $T = 0.3$  to  $27$  K. As evident in the curves at  $0.3$  and  $1.5$  K,  $R_0$  undergoes a very steep, divergent increase when  $H$  exceeds  $25$  T. The region just before the divergence occurs is shown in greatly expanded scale in the inset. At  $27$  K, the increase in  $R_0$  is relatively modest ( $\times 20$ ) between  $B = 0$  and  $31$  T (inset). However, as  $T$  decreases to  $5$  K, the increase steepens sharply, as reported [19] for K 7. Further cooling from  $5$  to  $0.3$  K changes the profile only very slightly. In the main panel,

the curves at  $0.3$  and  $1.5$  K (which cannot be distinguished) show that  $R_0$  diverges to  $40$  M  $\Omega$ , with a slope that steepens rapidly with  $H$ . The 3-decade increase ( $40$  k  $\Omega$  to  $40$  M  $\Omega$ ) occurs within the narrow interval  $17$ - $27$  T. We find that the observed divergence is too steep to fit a power-law of the kind  $R_0 \propto (H_c - H)^{-p}$ , with  $p > 0$  and  $H_c$  a critical field.

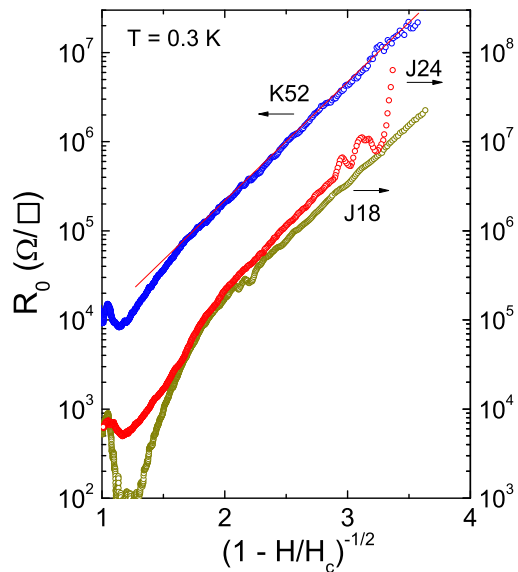


FIG. 2: (color online) Plot of  $R_0$  vs.  $(1 - H/H_c)^{-1/2}$  for Samples K 52, J18 and J24 at  $T = 0.3$  K, where  $h = H/H_c$  (the curve for K 52 is displaced by 1 decade for clarity).  $R_0$  is expressed as sheet resistance ( $\Omega/\square$ ). For each sample,  $H_c$  is the optimal value that gives the best straight-line fit vs.  $(1 - H/H_c)^{-1/2}$  (curvature is noticeable if  $H_c$  is altered by  $0.1$  T from this value). For Samples K 52, J18 and J24,  $H_c$  equals  $29.1, 32.1$  and  $35.5$  T, respectively. For K 52, the thin solid line is the expression  $R(h) = 440 \exp[b(1 - h)^{-1/2}]$ , with  $b = 1.54$ . The data match  $R(h)$  very well over nearly 3 decades in  $R_0$ .

As in Ref. [19], we compare the divergence with that predicted for the Kosterlitz-Thouless (KT) transition. In 2D systems described by the XY model, the ordered phase is destroyed at the KT transition by unbinding of pairs of topological excitations (e.g. vortices). As the transition here is induced by varying the applied field  $H$ , we replace the reduced temperature  $t$  by the reduced field  $h = H/H_c$ , with  $H_c$  the critical field. In the limit  $h \rightarrow 1$ , the KT correlation length diverges as

$$\xi = a \exp[b(1 - h)^{-1/2}]; \quad (1)$$

where  $a$  is the lattice parameter and  $b$  a number  $> 1$ .

The quality of the fit to Eq. 1 is best revealed in a plot of  $\log R_0$  vs. the quantity  $(1 - H/H_c)^{-1/2}$ . In Fig. 2,

we have plotted  $\log R_0$  in 3 samples K 52, J19 and J24 against  $1 - 1/h$ . In each sample, the value of  $H_c$  is adjusted to maximize the high-field portion of the plot that falls on a straight line (this is the only adjustment made). In Samples K 52, J18 and J24, the inferred values of  $H_c$  are 29.1, 32.1 and 35.5 T, respectively. The values of  $R_0$  in K 52 fit the straight line representing the expression  $R(h) = 440 \exp[2b(1 - h)]$ , with  $H_c = 29.1$  T and  $b = 1.54$ . The value of  $b$  is consistent with the KT transition. The 3-decade span is strong evidence that Eq. 1 accurately describes the divergence in  $R_0$ , and supports the inference that, at low  $T$ , we are observing a 2D KT-type phase transition to a high-field ordered state that is insulating.

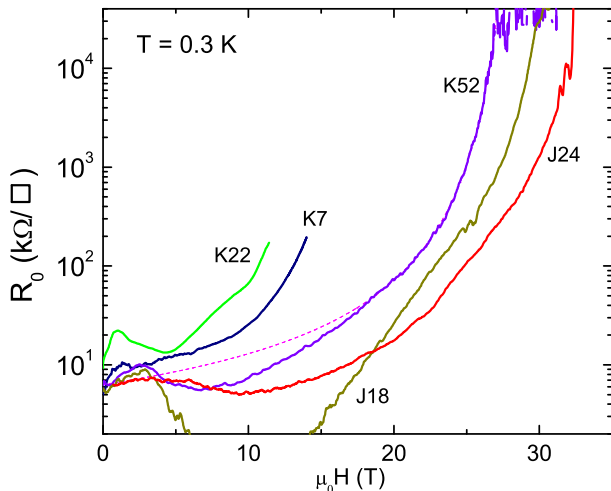


FIG. 3: (color online) Comparison of the curves of  $R_0$  vs.  $H$  at 0.3 K in log-log scale in 5 samples K 7, K 22, K 52, J18 and J24 with gate voltage offsets  $V_0 = 1, -0.6, 3, 20, 24$  V, respectively ( $V_0$  before annealing is not known in J18).  $R_0$  is expressed as sheet resistance  $\square$ . In K 7 and K 22 (which have small  $V_0$ ), the divergence in  $R_0$  occurs at a lower  $H$  [19]. The ferromagnetic-dissipation technique applied to K 52, J18 and J24 was not available for K 7 and K 22 (their curves were limited to  $R_0 < 0.3$  M $\square$ ). The dashed curve is the fit of the K 52 data to  $R$ .

The significant spread of  $H_c$  inferred from the fits in Fig. 2 is in accord with Ref. [19] which reported that  $H_c$  correlates with the offset voltage  $V_0$ . In Fig. 2, the samples K 52, J18 and J24 display a much larger critical field  $H_c$  than the sample K 7 (with  $V_0 = 1$  V and  $H_c = 18$  T) studied in detail in Ref. [19]. Figure 3 plots together, in log-log scale, the curves of  $R_0$  vs.  $H$  in the 5 samples for which we have detailed high-field transport results. The systematic shift to higher fields of the divergence (in the order K 22, K 7, K 52 and J24) is matched by the increase in their  $V_0$  (-0.5, 1, 3, 20 and 24 V, respectively). The value of  $V_0$  before annealing in J18 is not known. The dependence of  $H_c$  on  $V_0$  is non-linear. Initially (for  $0 < V_0 < 4$  V),  $H_c$  increases rapidly, but appears to increase rather slowly when  $V_0$  exceeds 20 V.

From a study of how  $V_0$  affects the zero-field transport,

we have obtained evidence that the zero-field mobility  $\mu_0$  is strongly suppressed if  $V_0$  is large. In Fig. 4, we display curves of  $R_{xx}$  vs. the unshifted gate voltage  $V_g$  in a batch of samples that includes K 22. The curves are taken at 295 K or 4 K (as indicated). In each sample, the width  $\Delta V_g$  of the peak at the Dirac point directly measures  $1 - \mu_0$ . Clearly, the width increases dramatically with  $V_0$ . These results support the inference that a large offset  $V_0$  gives rise to large electronic disorder which enhances disorder scattering and suppresses  $\mu_0$ . In turn, in an intense field, the transition field  $H_c$  is pushed to higher values. While these correlations do not exclude other factors that may influence  $H_c$ , we have found that  $V_0$  is the single most reliable predictor of the field scale at which the divergence onsets at low  $T$ .

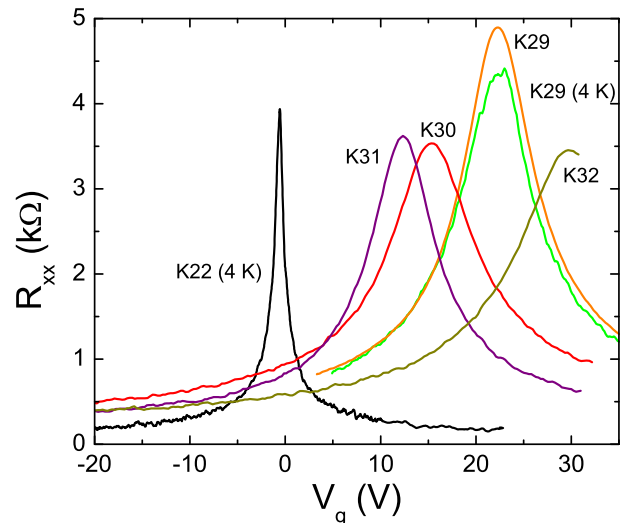


FIG. 4: Curves of the longitudinal resistance  $R_{xx}$  vs. unshifted gate voltage  $V_g$  in zero- $H$  in a series of samples at 295 K and 4 K (as indicated). The width of the peak in  $R_{xx}$  increases systematically with  $V_0$  (located by the peak position). This implies that the mobility  $\mu_0$  is very low in samples with large  $V_0$ .

#### IV. DOPING DEPENDENCE

Further insight into the nature of the divergence is obtained by viewing the behavior of the longitudinal resistance  $R_{xx}$  vs.  $V_g$  in a narrow gate window around the Dirac point at fixed  $B$  (with  $T$  kept at 0.3 K). Figure 5a displays a series of curves of  $R_{xx}$  (in log scale) vs.  $V_g$  in K 52 for fields  $10 \leq H \leq 31$  T. At 10 T,  $R_{xx}$  displays 3 well-separated peaks corresponding to  $n = 0$  LL at 20 V and the  $n = \pm 1$  LL's at 6 and 38 V, respectively. For  $H = 20$  T, the  $n = \pm 1$  levels move out of the gate-voltage window. We focus on the divergent enhancement of the central peak as  $B$  increases to 31 T. The key feature is that  $R_{xx}$  at the Dirac point ( $V_g = 20$  V) rises most rapidly especially for  $B > 25$  T.

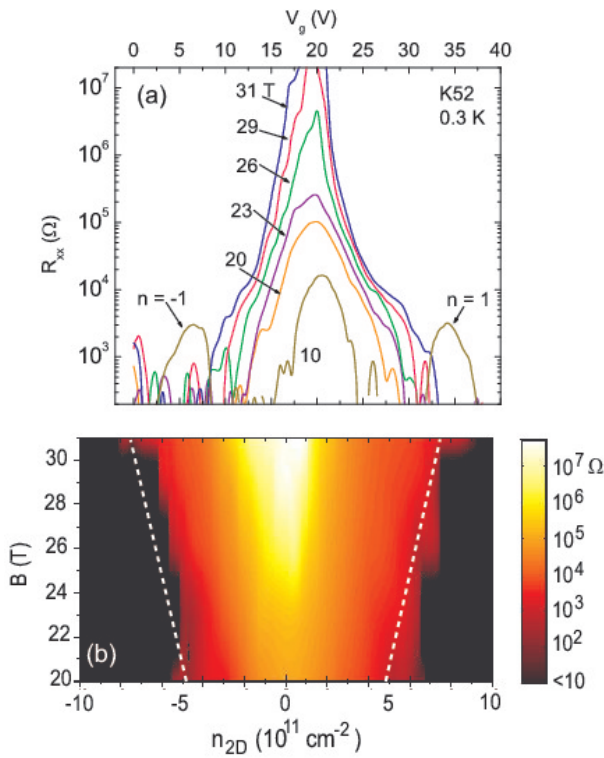


FIG. 5: (color online) Variation of  $R_{xx}$  (Sample K52) vs. the gate voltage  $V_g$  in the interval  $(0 < V_g < 38 \text{ V})$ , with  $B$  fixed at selected values 10 (31 T), and  $T = 0.3 \text{ K}$  (Panel a). At  $B = 10 \text{ T}$ , the central peak ( $n = 0$  LL) is well separated from the LL peaks labelled as  $n = 1$ . At  $B = 20 \text{ T}$  and higher, the  $n = 1$  LL's fall outside the gate window. With increasing  $B$ , the central peak increases rapidly and broadens. At the maximum  $B$  (31 T),  $R_{xx}$  at the Dirac point ( $V_g = 20 \text{ V}$ ) diverges to values above  $40 \text{ M}\Omega$ . The voltage-regulated technique has poor resolution when  $R_{xx}$  falls below  $0.3 \text{ k}\Omega$ . Panel (b) shows the contour plot of  $R_{xx}(n_{2D}; B)$  at  $0.3 \text{ K}$  in the  $n_{2D}$  ( $B$ ) plane (color bar of  $R_{xx}$  shown on right). The dashed lines trace the sublevel degeneracy  $1=2 \nu_B^2$ . The density is given by  $n_{2D} = CV_g/Ae$  where  $C$  and  $A$  are the capacitance and area of the device, respectively ( $C/A = 1.14 \times 10^{-4} \text{ Fm}^{-2}$ ).

It is instructive to view  $R_{xx}$  (at  $0.3 \text{ K}$ ) as a contour plot in the  $n_{2D}$  ( $B$ ) plane where  $n_{2D}$  is the 2D density of carriers doped by gating (Fig. 5b). The color bar (right) gives the magnitude of  $R_{xx}$ . Interestingly, the steep increase in  $R_{xx}$  with  $B$  is connected to the region between the dashed lines, which trace the sublevel degeneracy  $1=2 \nu_B^2$ . This suggests that only the states within the lowest sublevels (on either side of  $\nu = 0$ ) are affected by the opening of the gap. The contours appear to converge to a rounded cusp at  $n_{2D} = 0$ , but with a curvature that increases rapidly with  $B$ . At the largest  $R_{xx}$  (white region), the contour resembles a narrow, sharp wedge. The contour pattern suggests that  $H_c$  increases very rapidly from the value  $29.1 \text{ T}$ , as  $n_{2D}$  deviates from 0.

The physical picture implied by the results is that, at the Dirac point, a field-induced transition to a gapped, insulating state occurs at  $H_c$ . The value of  $H_c$  is highly

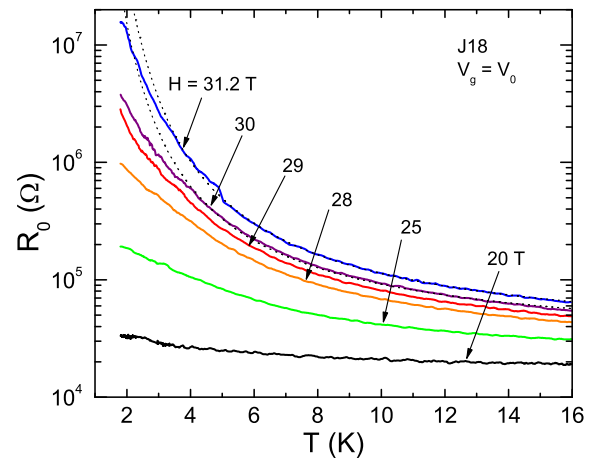


FIG. 6: (color online) The  $T$  dependence of  $R_0$  in Sample J18 with  $H$  fixed at selected values in the interval  $20 < H < 31.2 \text{ T}$ . As  $H$  approaches  $H_c$  ( $32.1 \text{ T}$ ),  $R_0$  approaches the thermally activated form  $e^{-T/\Delta}$ . The thin dashed curves are fits to this form with the gap  $\Delta = 12.9$  and  $14.7 \text{ K}$  at  $H = 30$  and  $31.2 \text{ T}$ , respectively. At the highest field ( $31.2 \text{ T}$ ),  $R_0$  increases by a factor of 310 between 16 and  $2 \text{ K}$ .

sensitive to slight deviations away from exact charge neutrality (Fig. 5). As we decrease  $H$  below  $H_c$ , the ordered state is unstable to the spontaneous unbinding of (vortex-like) topological excitations which have a mean spacing of  $(Eq. 1)$ . Because  $R_0$  fits accurately to  $e^{-T/\Delta}$  over 3 decades, we infer that the conduction scales as the density of excitations. Hence the excitations are charged, and they carry the entire current  $I$  in the limit  $T \rightarrow 0$ . As this conduction channel is qualitatively distinct from thermally activated carriers, it may account for the unusual "saturation" behavior of  $R_0$  vs.  $T$  [19]. As  $T \rightarrow 0$ , with  $H$  fixed near  $H_c$ , the conduction crosses over at  $1 \text{ K}$  from a steep, thermally activated channel to a  $T$ -independent channel carried by the excitations (Fig. 1b).

## V. TEMPERATURE DEPENDENCE

The  $T$  dependence of  $R_0$  in J18 with  $H$  fixed at selected values is displayed in semilog scale in Fig. 6. At the relatively high field  $H = 20 \text{ T}$ , the 2-fold increase in  $R_0$  between 16 and  $2 \text{ K}$  is quite modest. However, above  $20 \text{ T}$ , the  $T$  dependence steepens rapidly. As  $H$  is increased towards the critical  $H_c (= 32.1 \text{ T})$ , the profile of  $R_0$  moves ever closer to the activated form  $R_0 \sim e^{-T/\Delta}$ . We have plotted fits to the activated form (dashed curves) at the 2 highest fields  $H = 30$  and  $31.2 \text{ T}$ . At the highest  $H$ , the measured  $R_0$  tracks closely the dashed curve until  $T$  falls below  $3 \text{ K}$  where it deviates downwards. As  $H$  decreases further from  $H_c$ , the deviations start at a higher  $T$ . The gap value  $\Delta$  equals  $12.9$  and  $14.7 \text{ K}$  at  $30$  and  $31.2 \text{ T}$ , respectively. The latter provides an estimate of the energy gap in the ordered state for J18. Establishing that  $R_0$  is thermally activated when  $H > H_c$  is an essential goal, as

it shows that the ground state above  $H_c$  is a true insulator with a well-defined gap order parameter (as opposed to a state in which the carriers are strongly localized). Although the curves in Fig. 6 come close to establishing this result, measurements of  $R_0$  vs.  $T$  in samples with more accessible  $H_c$  are desirable.

Interestingly, throughout the pre-transition region ( $20 < H < H_c$ ),  $R_0$  also displays large increases with decreasing  $T$ . The carriers are strongly affected by the impending insulating state. We interpret these changes as reflecting very strong fluctuations in the order parameter that characterizes the ordered insulating phase. The strong  $T$  dependence is also apparent in the fixed- $T$  curves shown in Fig. 1.

Quite apart from the thermal activation argument, there are other evidence to suggest that the divergence is not consistent with electron localization. As evident from measuring the widths of the peaks of  $R_{xx}$  vs.  $V_g$  taken in zero  $B$ , samples with smallest  $|V_0|$  are the least disordered. The electron mobility  $\mu_e$  decreases from  $2.5$  to  $0.5 \text{ T}^{-1}$  as  $|V_0|$  increases from  $0.5$  to  $20 \text{ V}$ . With this trend in mind, we compare in Fig. 3 the profiles of  $R_0$  vs.  $B$  in K52 with K7 and K22 [19]. In Samples K22 and K7 (with  $V_0 = -0.6$  and  $1 \text{ V}$ , respectively), the divergence in  $R_0$  is apparent in relatively low  $B$  (below  $12 \text{ T}$ ). By contrast, we must go to much higher fields ( $> 20 \text{ T}$ ) in K52. The dashed line is the fit to  $R$  in K52 ( $H > 18 \text{ T}$ ) described above.

In the localization scenario, the observed divergence of  $R_0$  in strong field is explained by postulating that  $B$  induces localization of the electrons. However, applying this reasoning to the 3 samples in Fig. 3, we would conclude that a modest  $B$  is sufficient to trigger the localization in clean samples, but very intense fields are needed in dirtier samples. This implies that disorder and field act in opposition to bring about localization, which is in conflict with physical intuition. In addition, localization induced by  $B$  cannot lead to the singular divergence observed in  $R_0$  (Fig. 2). For these reasons, we believe that localization is not a viable explanation for the divergence in  $R_0$ .

## V I. D I S C U S S I O N

In the absence of Zeeman splitting and electron-electron interaction, the  $n = 0$  LL is 4-fold degenerate corresponding to the (physical) spin degeneracy indexed by  $s = 1$  and the  $K$  and  $K^0$  valley degeneracy indexed by  $v = 1$ . At  $\nu = 0$ , the energy of the  $n = 0$  LL,  $E_s$ , is zero. The effect of interaction in producing a broken-symmetry ground state has been investigated by several groups. To discuss our experiment, it is convenient to distinguish 2 different theoretical scenarios for the  $n = 0$  LL.

In one scenario, the Quantum Hall Ferromagnet (QHF) models, the exchange energy  $E_{ex} = \mu_B B$  leads to ferromagnetic polarization of the physical spins [7, 8, 10, 12,

17]. This produces a spin gap in the bulk without affecting the valley degeneracy, i.e.  $E = (\mu_B B + E_{ex})$  with  $\mu_B$  the Bohr magneton. Near the edge of the sample, the residual valley degeneracy is lifted by the edge potential. An important consequence of the QHF scenario at  $\nu = 0$  is the existence of spin-filtered counter-propagating edge (CPE) modes which result in a residual conductance of  $2e^2/h$  regardless of the magnitude of the spin gap in the bulk [12, 17, 18]. [In principle, the CPE modes are not present if the exchange polarizes instead the valleys to produce the bulk gap (this involves the same exchange energy  $E_{ex}$ ). However, most investigators favor the spin-polarization scenario in graphene because it is augmented by the Zeeman energy  $\mu_B B$  (the valley-polarization scenario is also called the QHF following the original usage [20] in quadratic, bilayer GAA s-based devices).]

In the second scenario, called magnetic catalysis [1, 13, 14, 15, 16], the field component  $B_z$  normal to the graphene sheet triggers electron-hole condensation. The instability introduces a mass term to the Dirac equation which leads to the order parameter [13, 14, 15]  $\chi = \int (j_A^\dagger j_B - j_B^\dagger j_A)$ , where  $\psi_A$  and  $\psi_B$  are the wave functions of electrons of spin and valley at sites A and B, respectively. The instability { a solid-state realization of chiral-symmetry breaking in (2+1)D [21] } results in preferential occupation of, say, the A sublattice sites over the B sites, and drives the system into an insulating state. Significantly, the instability is strongest for  $n = 0$ .

The steep increase in  $R_0$  vs.  $H$  first reported in Ref. [19] implies that at large  $H$ , the ground state at the Dirac point has a resistance at least 20 times larger than the quantum  $h/e^2$ . Although the measurements were limited to  $R_0 < 0.3 \text{ M}\Omega$ , the upturn appeared to diverge at a critical field  $H_c$ , suggestive of a singular field dependence. The findings are clearly at odds with the existence of CPE modes (see, however, the results in Ref. [18]).

In the present report, we have extended by a factor of 200 the range of resistance measurements and shown that, at  $0.3 \text{ K}$ , the increase in  $R_0$  is truly divergent as well as singular. Moreover, this behavior has been observed in all samples investigated to date by us in high fields. The evidence amassed clearly establish that the high-field ground state at the Dirac point is a true insulator (at least for samples prepared on a  $\text{SiO}_2$  substrate). In fact, the CPE modes do not exist in the insulating state. However, our results do not preclude them at low fields.

Lately, several groups have considered how the CPE modes are affected by intense field. A very interesting possibility is that an intense field destroys the CPE modes in a field-induced transition. It has been pointed out to us that the CPE modes are not protected against 2-particle exchange scattering with spin flip [22]. As the exchange energy increases with  $B$ , the increased scattering rate could lead to a gap in the edge modes.

In the magnetic catalysis scenario, Gorbar et al. [15] recently considered the competition between the mass gap  $\chi$  and the spin gap (augmented by Zeeman energy)

and inferred that CPE states exist only above a critical field  $B_{cr}$ .

Shinshoni et al. [23] have proposed that scattering of magnetic impurities can lead to strong localization of electrons in CPE modes which can mimic a KT transition. However, this scenario needs to be reconciled with the observed nearly activated behavior of  $R_0$  as well as the variation of  $H_c$  with  $V_0$  in different samples.

## VII. APPENDIX

Near the Dirac point, resistance traces are strongly distorted when the Ohmic heating  $P$  exceeds 10 pW at bath temperatures  $T_b$  below 1 K. As examples, we plot in Fig. 7 resistance traces (with  $I$  fixed). In Panel a, the inferred curve of  $R_{xx}$  vs.  $V_g$ , measured with  $B = 31$  T,  $I = 10$  nA and  $T = 0.3$  K, shows a pronounced dip near the Dirac point caused by selfheating instability (the true  $R_0$  exceeds 10 M $\Omega$ ). Panel b shows  $R_0$  vs  $B$  measured at fixed  $I$ . In the curve for K23 (at 5 K), selfheating reverses the trend of  $R_0$ . The downturn is avoided when  $I$  is decreased to 1 nA, but the measured curve (in K22 at 0.3 K) is still greatly suppressed from the true divergent profile.

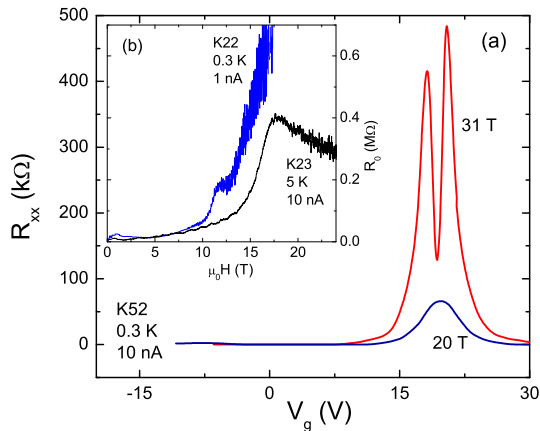


FIG. 7: (color online) Spurious features caused by sample selfheating in graphene. Panel (a) shows a gate-sweep measurement at  $T = 0.3$  K of  $R_{xx}$  vs.  $V_g$  in K52, with  $I$  fixed at 10 nA (dc). At  $B = 31$  T (red curve), severe selfheating inverts the peak at the Dirac point (as shown in Fig. 1,  $R_0$  actually exceeds 40 M $\Omega$ ). Heating effects are less severe in the 20-T curve. Panel (b) displays curves of  $R_0$  vs.  $B$  measured in Samples K22 (at 0.3 K) and K23 (at 5 K) with  $I$  fixed at 1 and 10 nA (dc), respectively. When  $R_0 > 0.2$  M $\Omega$ , selfheating produces the spurious shoulders and broad peaks, whose positions and shapes depend on  $I$ .

Figure 8 is a schematic of the measuring circuit employed in the ultralow-dissipation technique. A nominally constant ac voltage (40 V) of frequency 3 Hz is applied across the sample in series with a 100-k $\Omega$  buffer resistor. The current passing through the sample is measured by a Keithley picoammeter whose output is phase-

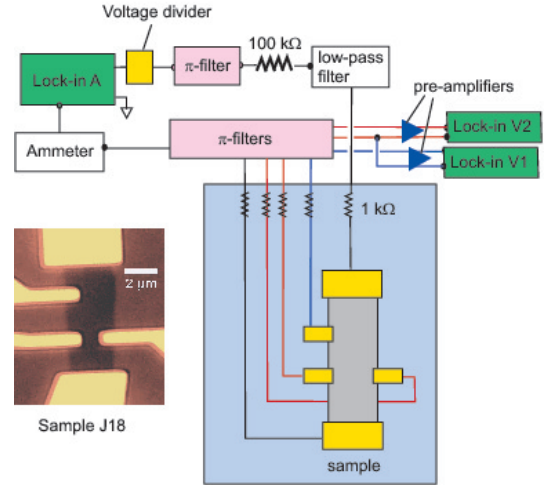


FIG. 8: (color online) Schematic of the low-dissipation, voltage-regulated circuit used in the experiment. Lock-in (amplifier) A produces a regulated voltage emf (3 Hz) that is reduced to an amplitude of 40 V by a 100:1 voltage divider. The signal goes through a  $\pi$ -filter, a buffer resistor (100 k $\Omega$ ) and a low-pass filter before entering the dewar. The AC current passing through the graphene sample is measured by the picoammeter (Keithley), whose output is phase-detected by Lock-in A. The longitudinal voltage  $V_{xx}$  and Hall voltage  $V_{xy}$  are phase-detected by Lock-ins  $V_1$  and  $V_2$ , respectively, after transmission through a bank of  $\pi$ -filters and high-impedance (100 M $\Omega$ ) pre-amplifiers. As shown, all wires entering the dewar are buffered by 1 k $\Omega$  nichrome thin-film ceramic resistors. The inset (lower left) shows Sample J18.

detected by the lock-in amplifier A. Simultaneously, the longitudinal voltage  $V_{xx}$  and Hall voltage  $V_{xy}$  are phase-detected by 2 other lock-ins. As shown, all wires entering the dewar are filtered and buffered to exclude extraneous RF signals which may be a potential source of sample heating.

Using the ultralow-dissipation technique, we completely avoid the thermal runaway problems illustrated in Fig. 7. At selected fields, we have performed I-V measurements to check that selfheating is not skewing the results even at our lowest  $T$  (0.3 K). Figure 9 shows curves of  $I$  vs.  $V_{xx}$  at the Dirac point in K52 at  $T = 0.3$  K with  $H$  fixed at 20 and 24 T. The linearity implies that selfheating is not observable up to a bias voltage of 2 mV. Since all the curves displayed in the main text were taken with a bias of 40 V, we are comfortably within the Ohmic regime.

We thank H. A. Fertig, P. A. Lee, D. Abanin, V. A. Miransky, E. Shinshoni, F. D. M. Haldane and D. N. Sheng for valuable comments, and acknowledge support from NSF-MRSEC under Grant DMR-0819860, and from the Princeton Center for Complex Materials. The experiments were performed at the National High Magnetic Field Laboratory, which is supported by NSF Co-

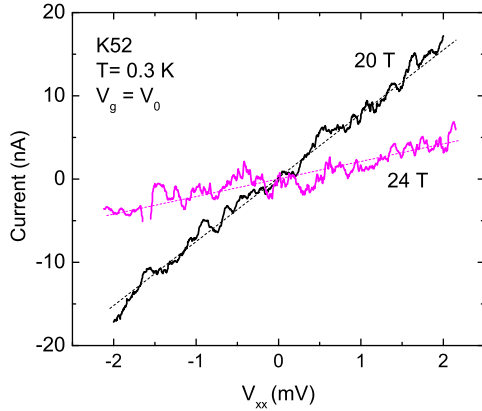


FIG. 9: (color online) The current-voltage curves measured at the Dirac Point ( $V_g = V_0$ ) in Sample K52 at  $T = 0.3$  K at the fields  $H = 20$  and  $24$  T (using the circuit in Fig. 8). The linearity of  $I$  vs.  $V_{xx}$  implies that, at these fields, self-heating is not observable at these power-dissipation levels (the dashed lines are guides to the eye).

operative Agreement No. DMR-084173, by the State of Florida, and by the Department of Energy.

Current address of LL: Dept. of Physics, MIT

- 
- [1] K. S. Novoselov, A. K. Geim, S. V. Morozov, D. Jiang, Y. Zhang, V. Dubonos, I. V. Grigorieva, A. A. Firsov, *Science* 306, 666-669 (2004).
- [2] K. S. Novoselov, D. Jiang, F. Schedin, T. J. Booth, V. V. Khotkevich, S. V. Morozov, A. K. Geim, *Proc. Natl. Acad. Sci. USA* 102, 10451-10453 (2005).
- [3] K. S. Novoselov, A. K. Geim, S. V. Morozov, D. Jiang, M. I. Katsnelson, I. V. Grigorieva, S. V. Dubonos, A. A. Firsov, *Nature* 438, 197-200 (2005).
- [4] Y. Zhang, J. Tan, H. L. Stormer and P. Kim, *Nature* 438, 201-204 (2005).
- [5] Y. Zhang, Z. Jiang, J. P. Small, M. S. Purewal, Y.-W. Tan, M. Fazlollahi, J. D. Chudow, J. A. Jaszczak, H. L. Stormer, P. Kim, *Phys. Rev. Lett.* 96, 136806 (2006).
- [6] Z. Jiang, Y. Zhang, H. L. Stormer and P. Kim, *Phys. Rev. Lett.* 99, 106802 (2007).
- [7] K. Nomura and A. H. MacDonald, *Phys. Rev. Lett.* 96, 256602 (2006).
- [8] J. Alicea and M. P. A. Fisher, *Phys. Rev. B* 74, 075422 (2006).
- [9] Kun Yang, S. DasSarma and A. H. MacDonald, *Phys. Rev. B* 74, 075423 (2006).
- [10] M. O. Goerbig, R. Moessner and B. Douçot, *Phys. Rev. B* 74, 161407(R) (2006).
- [11] Motohiko Ezawa, *J. Phys. Soc. Japan* 76, 094701 (2007).
- [12] D. A. Abanin, P. A. Lee and L. S. Levitov, *Phys. Rev. Lett.* 96, 176803 (2006).
- [13] D. V. Khveshchenko, *Phys. Rev. Lett.* 87, 206401 (2001).
- [14] V. P. Gusynin, V. A. Miransky, S. G. Sharapov and I. A. Shovkovy, *Phys. Rev. B* 74, 195429 (2006).
- [15] E. V. Gorbar, V. P. Gusynin and V. A. Miransky, *Low Temp. Phys.* 34, 790-793 (2008).
- [16] V. P. Gusynin, V. A. Miransky, S. G. Sharapov, and I. A. Shovkovy, *Phys. Rev. B* 77, 205409 (2008).
- [17] H. A. Fertig and L. Brey, *Phys. Rev. Lett.* 97, 116805 (2006).
- [18] Dmitry A. Abanin, Kostya S. Novoselov, Uli Zeitler, Patrick A. Lee, A. K. Geim, and L. S. Levitov *Phys. Rev. Lett.* 98, 196806 (2007).
- [19] Joseph G. Checkelsky, Lu Li, and N. P. Ong, *Phys. Rev. Lett.* 100, 206801 (2008).
- [20] K. Moon, H. Mori, Kun Yang, S. M. Girvin, A. H. MacDonald, L. Zheng, D. Yoshioka, and Shou-Cheng Zhang, *Phys. Rev. B* 51, 5138 (1995).
- [21] V. P. Gusynin, V. A. Miransky, and I. A. Shovkovy, *Phys. Rev. Lett.* 73, 3499 (1994); *Phys. Rev. D* 52, 4718 (1995).
- [22] F. D. M. Haldane and D. N. Sheng, private communication.
- [23] E. Shimshoni, H. A. Fertig, and G. Venkateswara Pai, *cond-mat.arXiv:0807.2867v1*.